REPORT DOCUMENTATION PAGE

Form Approved OMB NO. 0704-0188

1. REPORT DATE (DD-MM-YYYY)	2. REPORT TYPE	3. DATES COVERED (From - To)
	New Reprint	-

4. TITLE AND SUBTITLE

Thermal radiation of lamellar metal-dielectric metamaterials and metallic surfaces

5a. CONTRACT NUMBER
W911NF-14-1-0639

5b. GRANT NUMBER

5c. PROGRAM ELEMENT NUMBER
611102

6. AUTHORS

M. A. Noginov, A. Mozafari, T. U. Tumkur, J. K. Kitur, E. E. Narimanov

5d. PROJECT NUMBER

5e. TASK NUMBER

5f. WORK UNIT NUMBER

7. PERFORMING ORGANIZATION NAMES AND ADDRESSES

Norfolk State University
700 Park Avenue
McDemmond Center for Applied Research, Suite 601
Norfolk, VA 23504 -8060

8. PERFORMING ORGANIZATION REPORT NUMBER

9. SPONSORING/MONITORING AGENCY NAME(S) AND ADDRESS (ES)

U.S. Army Research Office
P.O. Box 12211
Research Triangle Park, NC 27709-2211

10. SPONSOR/MONITOR'S ACRONYM(S)
ARO

11. SPONSOR/MONITOR'S REPORT NUMBER(S)
63748-PH-H.2

12. DISTRIBUTION AVAILIBILITY STATEMENT

Approved for public release; distribution is unlimited.

13. SUPPLEMENTARY NOTES

The views, opinions and/or findings contained in this report are those of the author(s) and should not contrued as an official Department of the Army position, policy or decision, unless so designated by other documentation.

14. ABSTRACT

We studied angular distributions and spectra of thermal radiation of lamellar metal/dielectric metamaterials with hyperbolic dispersion and compared them with the corresponding characteristics of simple metallic films and pairs of metallic and dielectric layers. The spectra of thermal radiation, in the mid-infrared part of the spectrum, were nearly flat and featureless, in a good agreement with the model predictions. The angular distributions of thermal emission deviated from the predictions of the Kirchoff's law and closely followed the Lambert's law, ?cos?. The thermal radiation properties of hyperbolic metamaterials were not much different from those of simpler metallic

15. SUBJECT TERMS

Metamaterials; Thermal Radiation

16. SECURITY CLASSIFICATION OF:			17. LIMITATION OF ABSTRACT	15. NUMBER OF PAGES	19a. NAME OF RESPONSIBLE PERSON
a. REPORT	b. ABSTRACT	c. THIS PAGE			Mikhail Noginov
UU	UU	UU	UU		19b. TELEPHONE NUMBER 757-823-2204

Report Title

Thermal radiation of lamellar metal-dielectric metamaterials and metallic surfaces

ABSTRACT

We studied angular distributions and spectra of thermal radiation of lamellar metal/dielectric metamaterials with hyperbolic dispersion and compared them with the corresponding characteristics of simple metallic films and pairs of metallic and dielectric layers. The spectra of thermal radiation, in the mid-infrared part of the spectrum, were nearly flat and featureless, in a good agreement with the model predictions. The angular distributions of thermal emission deviated from the predictions of the Kirchoff's law and closely followed the Lambert's law, ?cos?. The thermal radiation properties of hyperbolic metamaterials were not much different from those of simpler metallic structures.

REPORT DOCUMENTATION PAGE (SF298)
(Continuation Sheet)

Continuation for Block 13

ARO Report Number 63748.2-PH-H
Thermal radiation of lamellar metal-dielectric me...

Block 13: Supplementary Note

Approved for public release; distribution is unlimited.

Thermal radiation of lamellar metal-dielectric metamaterials and metallic surfaces

M. A. Noginov,[1*] A. Mozafari,[1] T. U. Tumkur,[1] J. K. Kitur,[1] and E. E. Narimanov[2]

[1] *Center for Materials Research, Norfolk State University, Norfolk, VA 23504, USA*
[2] *Birck Nanotechnology Center, Department of Electrical and Computer Engineering, Purdue University, West Lafayette, IN 47907, USA*
**mnoginov@nsu.edu*

Abstract: We studied angular distributions and spectra of thermal radiation of lamellar metal/dielectric metamaterials with hyperbolic dispersion and compared them with the corresponding characteristics of simple metallic films and pairs of metallic and dielectric layers. The spectra of thermal radiation, in the mid-infrared part of the spectrum, were nearly flat and featureless, in a good agreement with the model predictions. The angular distributions of thermal emission deviated from the predictions of the Kirchoff's law and closely followed the Lambert's law, $\propto\cos\theta$. The thermal radiation properties of hyperbolic metamaterials were not much different from those of simpler metallic structures.

OCIS codes: (160.3918) Metamaterials, (260.3060) Infrared, (290.6815) Thermal emission.

References

1. Planck's law, http://en.wikipedia.org/wiki/Planck's_law.
2. Radiative Equillibrium, http://en.wikipedia.org/wiki/Radiative_equilibrium.
3. P. Prevost, "Mémoire sur l'equilibre du feu," J. Phys. **38**, 314–322 (1791).
4. P. Prevost, (1791) "Memoir on the Equilibrium of Heat" in *The Laws of Radiation and Absorption: Memoirs by Prévost, Stewart, Kirchhoff, and Kirchhoff and Bunsen*, translated and edited by D. B. Brace (American Book Company, 1901).
5. B. Stewart, "An account of some experiments on radiant heat, involving an extension of the Prevot's theory of exchanges," Transactions of the Royal Society of Edinburgh, Vol. **XXII**, part I (1858); reprinted in *The Laws of Radiation and Absorption: Memoirs by Prévost, Stewart, Kirchhoff, and Kirchhoff and Bunsen*, translated and edited by D. B. Brace (American Book Company, 1901).
6. H. von Helmholtz, *Handbuch der physiologischen Optik*, *Allgemeinen Encyclopädie der Physik (*Leopold Voss, 1857), Volume 9.
7. G. G. Stokes, "On the perfect blackness of the central spot in Newton's rings, and on the verification of Fresnel's formulae for the intensities of reflected and refracted rays," Cambridge and Dublin Mathematical Journal, Vol. **IV**, 1–14 (1849); reprinted in *Physical and Mathematical Papers*, Vol. **II**, G. G. Stokes, ed., (Cambridge University Press, 1983).
8. G. R. Kirchhoff, "Über die Fraunhofer'schen Linien," 662–665 (1859) in *Monatsberichte der Königlich Preussischen Akademie der Wissenschaften zu Berlin* (Buchdruckerei der Königlichen Academie der Wissenschaften, 1875).
9. G. R. Kirchhoff, "Über den Zusammenhang zwischen Emission und Absorption von Licht und Wärme," 783–787 (1859) in *Monatsberichte der Königlich Preussischen Akademie der Wissenschaften zu Berlin* (Buchdruckerei der Königlichen Academie der Wissenschaften, 1875).
10. G. Kirchhoff, ""Ueber das Verhältniss zwischen dem Emissionsvermögen und dem Absorptionsvermögen der Körper für Wärme and Licht," Annalen der Physik und Chemie 109 (2), 275–301 (1860). "On the relation between the radiating and absorbing powers of different bodies for light and heat," Philosophical Magazine and Journal of Science, Series 4, Vol **20**, 1–21 (1860).
11. S. Chandrasekhar, S., *Radiative Transfer* (Dover Publications, 1960).
12. E. A. Milne, "Thermodynamics of the stars," in *Handbuch der Astrophysik* (Springer, 1930), 65–255 .
13. G. B. Rybicki and A. P. Lightman, *Radiative Processes in Astrophysics* (John Wiley & Sons, 1979).
14. D. Mihalas and B. Weibel-Mihalas, *Foundations of Radiation Hydrodynamics* (Oxford University Press, 1984).
15. R. M. Goody and Y. L. Yung, *Atmospheric Radiation: Theoretical Basis*, 2nd edition (Oxford University Press, 1989).
16. H. Kangro, *Early History of Planck's Radiation Law* (Taylor & Francis, 1976).
17. J. Tyndall, "Über leuchtende und dunkle Strahlung," Annalen der Physik und Chemie **200**(1), 36–53 (1865).

#231431 Received 24 Dec 2014; revised 12 Mar 2015; accepted 13 Mar 2015; published 4 Jun 2015

18. J. Tyndall, *Heat considered as a Mode of Motion* (D. Appleton & Company, 1869).
19. Crova, A.P.P, (1880). "Étude des radiations émises par les corps incandescents. Mesure optique des hautes temperatures," Annales de chimie et de physique, Série 5, vol. **19**, 472–550 (1880).
20. O. Lummer and F. Kurlbaum, "Der electrisch geglühte "absolut schwarze" Körper und seine Temperaturmessung," Verhandlungen der Deutschen Physikalischen Gesellschaft **17**, 106–111 (1898).
21. O. Lummer and F. Kurlbaum, "Der elektrisch geglühte "schwarze" Körper," Annalen der Physik **5**(8), 829–836 (1901).
22. F. Paschen, "Über Gesetzmäßigkeiten in den Spectren fester Körper und über ein neue Bestimmung der Sonnentemperatur," in *Nachrichten von der Königlichen Gesellschaft der Wissenschaften zu Göttingen (Mathematisch-Physikalische Klasse)* 294–304 (1895).
23. M. Planck "Über eine Verbesserung der Wienschen Spektralgleichung". Deutsche Physikalische Gesellschaft. Verhandlungen **2**, 202–204 (1900). Translated in D. ter Haar, "On an Improvement of Wien's Equation for the Spectrum", *The Old Quantum Theory*, 79–81 (Pergamon Press, 1967).
24. H. Rubens and F. Kurlbaum, "Über die Emission langer Wellen durch den schwarzen Körper," Verhandlungen der Deutschen Physikalischen Gesellschaft **2**, 181 (1900).
25. M. Planck, "Zur Theorie des Gesetzes der Energieverteilung im Normalspektrum," Verhandlungen der Deutschen Physikalischen Gesellschaft **2**, 237 (1900). Translated in D. ter Haar, "On the Theory of the Energy Distribution Law of the Normal Spectrum" in *The Old Quantum Theory*, 82. (Pergamon Press, 1967).
26. A. Einstein, "Über einen die Erzeugung und Verwandlung des Lichtes betreffenden heuristischen Gesichtspunkt". Annalen der Physik **17**(6), 132–148 (1905). Translated in D. ter Haar, "On an heuristic point of view about the creation and conversion of light", *The Old Quantum Theory*, 91–107 (Pergamon Press, 1967).
27. W. C. Snyder, Z. Wan, and X. Li, "Thermodynamic constraints on reflectance reciprocity and Kirchhoff's law," Appl. Opt. **37**(16), 3464–3470 (1998).
28. A. Kuznetsov, I. Melnikova, D. Pozdnyakov, O. Seroukhova, and A. Vasilyev, *Remote Sensing of the Environment and Radiation Transfer: An Introductory Survey* (Springer, 2012).
29. S. Y. Lin, J. Moreno, and J. G. Fleming, "Three-dimensional photonic-crystal emitter for thermal photovoltaic generation," Appl. Phys. Lett. **83**(2), 380–382 (2003).
30. E. Rephaeli and S. Fan, "Thermophotovoltaics: Absorber and emitter for solar thermophotovoltaic systems to achieve efficiency exceeding the Shockley-Queisser limit," Opt. Express **17**, 15145 (2009).
31. X. Liu, T. Tyler, T. Starr, A. F. Starr, N. M. Jokerst, and W. J. Padilla, "Taming the blackbody with infrared metamaterials as selective thermal emitters," Phys. Rev. Lett. **107**(4), 045901 (2011).
32. C. Wu, B. Neuner III, J. John, A. Milder, B. Zollars, S. Savoy, and G. Shvets, "Metamaterial-based integrated plasmonic absorber/emitter for solar thermo-photovoltaic systems," J. Opt. **14**(2), 024005 (2012).
33. S. Fan, S. Sandhu, Z. Yu, A. P. Raman, L. Zhu, and M. Anoma, "Thermal radiation control: enhancement of solar sell performance and daytime radiative cooling," presented at the SPIE Optics + Photonics, paper 9160–34, San Diego, CA, USA, 17–21 August 2014.
34. M. A. Noginov and V. A. Podolskiy, eds., *Tutorials in Metamaterials* (Taylor & Francis, 2011).
35. C.-M. Wang, Y.-C. Chang, M.-W. Tsai, Y.-H. Ye, C.-Y. Chen, Y.-W. Jiang, Y.-T. Chang, S.-C. Lee, and D. P. Tsai, "Reflection and emission properties of an infrared emitter," Opt. Express **15**(22), 14673–14678 (2007).
36. J. A. Mason, S. Smith, and D. Wasserman, "Strong absorption and selective thermal emission from a mid-infrared metamaterial," Appl. Phys. Lett. **98**(24), 241105 (2011).
37. P. A. Belov, R. Marqués, S. I. Maslovski, I. S. Nefedov, M. Silveirinha, C. R. Simovski, and S. A. Tretyakov, "Strong spatial dispersion in wire media in the very large wavelength limit," Phys. Rev. B **67**(11), 113103 (2003).
38. D. R. Smith and D. Schurig, "Electromagnetic wave propagation in media with indefinite permittivity and permeability tensors," Phys. Rev. Lett. **90**(7), 077405 (2003).
39. Z. Jacob, L. V. Alekseyev, and E. Narimanov, "Optical Hyperlens: Far-field imaging beyond the diffraction limit," Opt. Express **14**(18), 8247–8256 (2006).
40. A. Salandrino and N. Engheta, "Far-field subdiffraction optical microscopy using metamaterial crystals: Theory and simulations," Phys. Rev. B **74**(7), 075103 (2006).
41. Z. Liu, H. Lee, Y. Xiong, C. Sun, and X. Zhang, "Far-field optical hyperlens magnifying sub-diffraction-limited objects," Science **315**(5819), 1686 (2007).
42. S. Thongrattanasiri and V. A. Podolskiy, "Hypergratings: nanophotonics in planar anisotropic metamaterials," Opt. Lett. **34**(7), 890–892 (2009).
43. S. Ishii, A. V. Kildishev, E. Narimanov, V. M. Shalaev, and V. P. Drachev, "Sub-wavelength interference pattern from volume plasmon polaritons in a hyperbolic medium," Laser Photonics Review **7**(2), 265–271 (2013).
44. Z. Jacob, I. Smolyaninov, and E. E. Narimanov, "Broadband Purcell effect: Radiative decay engineering with metamaterials," Appl. Phys. Lett. **100**(18), 181105 (2012).
45. M. A. Noginov, H. Li, Y. A. Barnakov, D. Dryden, G. Nataraj, G. Zhu, C. E. Bonner, M. Mayy, Z. Jacob, and E. E. Narimanov, "Controlling spontaneous emission with metamaterials," Opt. Lett. **35**(11), 1863–1865 (2010).
46. J. Kim, V. P. Drachev, Z. Jacob, G. V. Naik, A. Boltasseva, E. E. Narimanov, and V. M. Shalaev, "Improving the radiative decay rate for dye molecules with hyperbolic metamaterials," Opt. Express **20**(7), 8100–8116 (2012).
47. L. Gu, T. U. Tumkur, G. Zhu, and M. A. Noginov, "Blue shift of spontaneous emission in hyperbolic metamaterial," Sci Rep **4**, 4969 (2014).

#231431 Received 24 Dec 2014; revised 12 Mar 2015; accepted 13 Mar 2015; published 4 Jun 2015

48. L. Gu, J. E. Livenere, G. Zhu, T. U. Tumkur, H. Hu, C. L. Cortes, Z. Jacob, S. M. Prokes, and M. A. Noginov, "Angular distribution of emission from hyperbolic metamaterials," Sci Rep **4**, 7327 (2014).
49. E. E. Narimanov and I. I. Smolyaninov, "Beyond Stefan-Boltzmann Law: Thermal Hyper-Conductivity", arXiv:1109.5444v1 [physics.optics] 26 Sept. 2011.
50. C. Simovski, S. Maslovski, I. Nefedov, and S. Tretyakov, "Optimization of radiative heat transfer in hyperbolic metamaterials for thermophotovoltaic applications," Opt. Express **21**(12), 14988–15013 (2013).
51. Y. Guo and Z. Jacob, "Thermal hyperbolic metamaterials," Opt. Express **21**(12), 15014–15019 (2013).
52. M. A. Kats, R. Blanchard, S. Zhang, P. Genevet, C. Ko, S. Ramanathan, and F. Capasso, "Vanadium dioxide as a natural disordered metamaterial: perfect thermal emission and large broadband negative differential thermal emittance," Phys. Rev. X **3**, 041004 (2013).
53. M. V. Klein and T. E. Furtak, *Optics* (Wiley 1986).
54. R. Siegel, *Thermal Radiation Heat Transfer* (CRC Press, 2001).
55. V. M. Shalaev, W. Cai, U. K. Chettiar, H.-K. Yuan, A. K. Sarychev, V. P. Drachev, and A. V. Kildishev, "Negative index of refraction in optical metamaterials," Opt. Lett. **30**(24), 3356–3358 (2005).
56. K.-P. Chen, V. P. Drachev, J. D. Borneman, A. V. Kildishev, and V. M. Shalaev, "Drude relaxation rate in grained gold nanoantennas," Nano Lett. **10**(3), 916–922 (2010).
57. S. M. Rytov, "Electromagnetic properties of a finely stratified medium," Sov. Phys. JETP **2**, 466–475 (1956).
58. J. E. Sipe and R. W. Boyd, "Nanocomposite materials for nonlinear optics based on local field effects," in *Optical Properties of Nanostructured Random Media*, V. M. Shalaev, ed. (Springer, 2002).
59. M. J. Weber, *Handbook of Optical Materials* (CRC Press, 2003).
60. N. Kaiser, A. Zuber, and U. Kaiser, "Evaluation of thin MgF_2 films by spectroscopic ellipsometry," Thin Solid Films **232**(1), 16–17 (1993).
61. M. A. Noginov, Y. A. Barnakov, G. Zhu, T. Tumkur, H. Li, and E. E. Narimanov, "Bulk photonic metamaterial with hyperbolic dispersion," Appl. Phys. Lett. **94**(15), 151105 (2009).
62. F. E. Nicodemus, "Directional reflectance and emissivity of an opaque surface," Appl. Opt. **4**(7), 767 (1965).

1. Introduction

The phenomenon of thermal radiation, which has been actively studied starting from the end of the eighteen's century, has played a pivotal role in the progress of physics and led to the notion of quantization of energy and emergence of quantum mechanics. The milestones of this intriguing development as well as the basic concepts, which are directly related to the present study, are briefly outlined below [1,2].

In 1791, Pierre Prevost showed that all bodies radiate heat and concluded that radiation should exactly compensate absorption [3,4]. In 1858, Balfour Stewart has reported his studies of thermal emission and absorption of various polished substrates, which he compared with that of a black soot (lamp black) – one of the darkest materials up to date [5]. His experiments, which he analyzed in terms of reflected and refracted beams obeying Helmholtz reciprocity principle [6] (also known as Stokes-Helmholtz reversion-reciprocity principle [6,7]), has led him to the conclusion of equality of (spectrally) selective emission and absorption at thermal equilibrium.

In 1859 and 1860, Gustav Robert Kirchhoff, not knowing of Steward's works [1], has published three papers on his studies of the emission and absorption of arbitrary bodies and their relation to the emission of a perfectly black body that absorbs 100% of incident light [8–10]. The Kirchhoff's law of thermal radiation, which is of key importance to the present study, states that for any material, radiating and absorbing in thermodynamic equilibrium at any given temperature T for every wavelength λ, the ratio of emissive power to an absorptance (the ratio between the absorbed power and the incident power) has one universal value, which is an emissive power of a perfect black body, $B(\lambda,T)$ [10–15]. Kirchhoff considered determination of the function $B(\lambda,T)$ to be the problem of the highest importance. However, finding the dependence of B on λ and T took four decades of experimental efforts and development of measurement techniques [1,16–22].

In 1900, Max Planck has proposed the empirical formula $B(\lambda,T)=\frac{C\lambda^{-5}}{\exp(c/k_BT)-1}$ [23], which had a very good agreement with the experimental data [24]. In his first formulation of the celebrated Planck's black body radiation law, C and c were empirical coefficients, and k_B was the Boltzmann's constant. Planck has further related the constant c (which should not be confused with the speed of light) to a quantum of energy e that was proportional to the

#231431 Received 24 Dec 2014; revised 12 Mar 2015; accepted 13 Mar 2015; published 4 Jun 2015

frequency v and the universal constant of nature h (now known as the Planck's constant), $e = hv$ [25]. Subsequently, Planck's law of black-body radiation contributed to the Einstein's concept of quanta of light [26], which explained photoluminescence, photoelectric effect, and ionization of gases by ultraviolet light and laid the basis for the development of quantum mechanics.

The Kirchhoff's law was first formulated for emission powers radiated by bodies in all directions. It has been further reformulated to take into account directionality of thermal radiation: emissivity in a given direction, $\varepsilon(\lambda,\varphi,\theta,\phi)$, is equal to the absorptance for radiation incident from that direction, $\alpha(\lambda,\varphi,\theta,\phi)$, which is equal (for opaque bodies) to one minus the directional reflectance for that same direction, 1-ρ(λ,φ,θ,ϕ) [27]. (Here emissivity $\varepsilon(\lambda,\varphi,\theta,\phi)$ is defined as the ratio of the emissive power of a material $E(\lambda,\varphi,\theta,\phi,T)$ to that of a perfect black body $B(\lambda,\varphi,\theta,\phi,T)$, φ is polarization, and θ and ϕ are the polar coordinates.) As ideal black body absorbs all radiation incident on it from any direction, and the thermal radiation power emitted by a small area dA into a small solid angle in the direction (θ,ϕ) is proportional to the projection of the area dA onto the plane perpendicular to this direction, the emissive power of a perfect black body is described by the Lambertian law $B(\theta) \propto \cos\theta$ [28].

As energy consumption worldwide ramps up year after year, management, generation, and disposal of heat radiation become increasingly important. Of particular interest to production of 'green' renewable energy is engineering of absorbing and radiating surfaces for thermo-photovoltaics, in particular, the structures with spectrally narrow thermal emission bands in the infrared part of the spectrum [29–32]. A similar concept of tailoring the spectrum of thermal radiation can also be applied to another important 'green' technology problem – radiation cooling [33].

Over last decade, an efficient control of heat radiation and absorption became possible due to the development of metamaterials [34] – engineered composite media based on subwavelength inclusions with rationally designed shapes, sizes and mutual orientations, embedded in dielectric hosts or arranged on materials' surfaces (metasurfaces). A combination of fundamental understanding of underlying physical processes and availability of sophisticated nanofabrication and modeling tools has allowed researchers to design and fabricate surfaces with tailored narrow absorption bands in the mid-infrared part of the spectrum [31,35,36]. In a good agreement with the Kirchhoff's law of thermal radiation, strengths, spectral positions, and shapes of the experimental thermal radiation bands have been shown to match those of the absorption bands [31,35,36]. In line with the directional form of the Kirchhoff's law, a good agreement between the experimental and the theoretically predicted angular distributions of thermal radiation has been demonstrated in Ref [36], in which the angular emission diagrams, measured between + 45° and –45°, were fairly flat.

Metamaterials with hyperbolic dispersion, in which dielectric permittivities in orthogonal directions have opposite signs [37–40], can propagate waves with nearly infinitely large wave-vectors [39,40], provide for far-field [39–41] and near-field [42,43] subdiffraction imaging, and have a broadband singularity of the density of photonic states [44]. They can control the rate [44–46], the spectra [47], and the directionality [44,48] of spontaneous emission of dye molecules and quantum dots. Furthermore, they can enhance propagation of thermal radiation inside the medium [49], facilitate near-field (micron range) heat transfer between two media [50], and enable super-planckian thermal energy transfer over a nanoscale air gap [51].

At the same time, far field spectra and angular distribution of thermal emission in hyperbolic metamaterials have never been researched. This gap of knowledge has motivated our studies of thermal radiation of lamellar metal-dielectric metamaterials and simpler metallic systems.

The paper is organized as follows. Following Introduction, the experimental samples and setups are described in Section 2. The results of the studies of angular distribution of thermal

#231431 Received 24 Dec 2014; revised 12 Mar 2015; accepted 13 Mar 2015; published 4 Jun 2015

radiation as well as thermal radiation spectra are reported in Section 3. These are the most important findings of this work. Section 3 has also a description of the room temperature reflectance measurements. The experimental results are compared to the model predictions in Section 4. The major results and conclusions are discussed and recapped in the Section 5.

2. Experimental samples and setup

2.1 Experimental samples

The core of the heater system in our studies was a modified solder iron (40 W from Weller), as discussed below. The experimental samples – thermally radiating metallic films and multilayered metal/dielectric stacks – were deposited onto a flat end of the 6 mm diameter copper-based solder iron rod, which was polished to a mirror shine, Fig. 1(a). A bare polished surface of the solder iron rod was used in thermal measurements as well (referred below as Cu sample). All thin film samples, including lamellar Au/MgF_2 metamaterial (consisting of seven 25 nm Au layers and six 35 nm MgF_2 layers), Au film on top of Cu, MgF_2 film on top of Cu, and MgF_2 film on top of Au film, have been fabricated using the thermal vapor deposition setup (Model 360A from Edwards and Nano 36 from Kurt J. Lesker). The "witness" samples were deposited onto glass substrates positioned in the thermal deposition apparatus in immediate proximity to the solder iron rods. They were used to measure the film thickness, with the help of the profilometer (Dektak XT from Bruker). Multiple samples of the same type have been fabricated and studied. The corresponding film thicknesses are reported in the text below as appropriate.

Thermal emission of the metallic-based samples was compared to that of black soot (lamp black), which has ≈96% emissivity in a broad spectral range [52] and whose thermal emission spectrum closely approximates that of a black body. Black soot was deposited on the flat end of the solder iron rod by using a candle.

2.2 Angular reflection profiles

Angular reflection profiles in p and s polarization have been studied in the Lambda 900 spectrophotometer equipped with the polarizer and 150 mm InGaAs integrating sphere (from Perkin Elmer). The sample (deposited on glass) was mounted in the rotating sample holder and was 5 cm long, in order to accommodate large incidence angles.

2.3 Heater and temperature control

Each of multiple interchangeable solder iron rods (with or without film coating) was mounted in such a way that the flat end (thermal radiation surface) was facing out, Figs. 1(a) and 1(b). A hole, 3 mm dip and 0.75 mm in diameter, was drilled in the side wall of the rod ~2.5 mm away from the sample surface, Figs. 1(a) and 1(b). A chromel-alumel thermocouple (K type, from OMEGA Engineering) was inserted into the hole to monitor the sample's temperature, Figs. 1(a) and 1(b). The voltage supplied to the solder iron was controlled by the auto-transformer, which allowed one to tune the temperature from room temperature to ~480 °C.

In our experiments, we studied thermal emission radiated by the flat end of the solder iron rod (with appropriate coating), and the heat generated by all other parts of the solder iron was an unwanted noise.

2.4 Angular emission setup

In the angular thermal radiation experiment described below, in order to screen the unwanted radiation from the detector, the solder iron was placed inside of a cylindrical metallic drum (155 mm in diameter and 132 mm in length) with metallic wall covering one of its bases, while the other base of the cylinder was open, Fig. 1(a). The hole, whose diameter was ~0.5 mm larger than the diameter of the solder iron rod, was drilled in the center of the base wall, and the solder iron was installed in such a way that the flat surface of the rod was flash with

#231431 Received 24 Dec 2014; revised 12 Mar 2015; accepted 13 Mar 2015; published 4 Jun 2015

the base of the cylinder, and the measures were taken for the rod not to touch the metal of the drum.

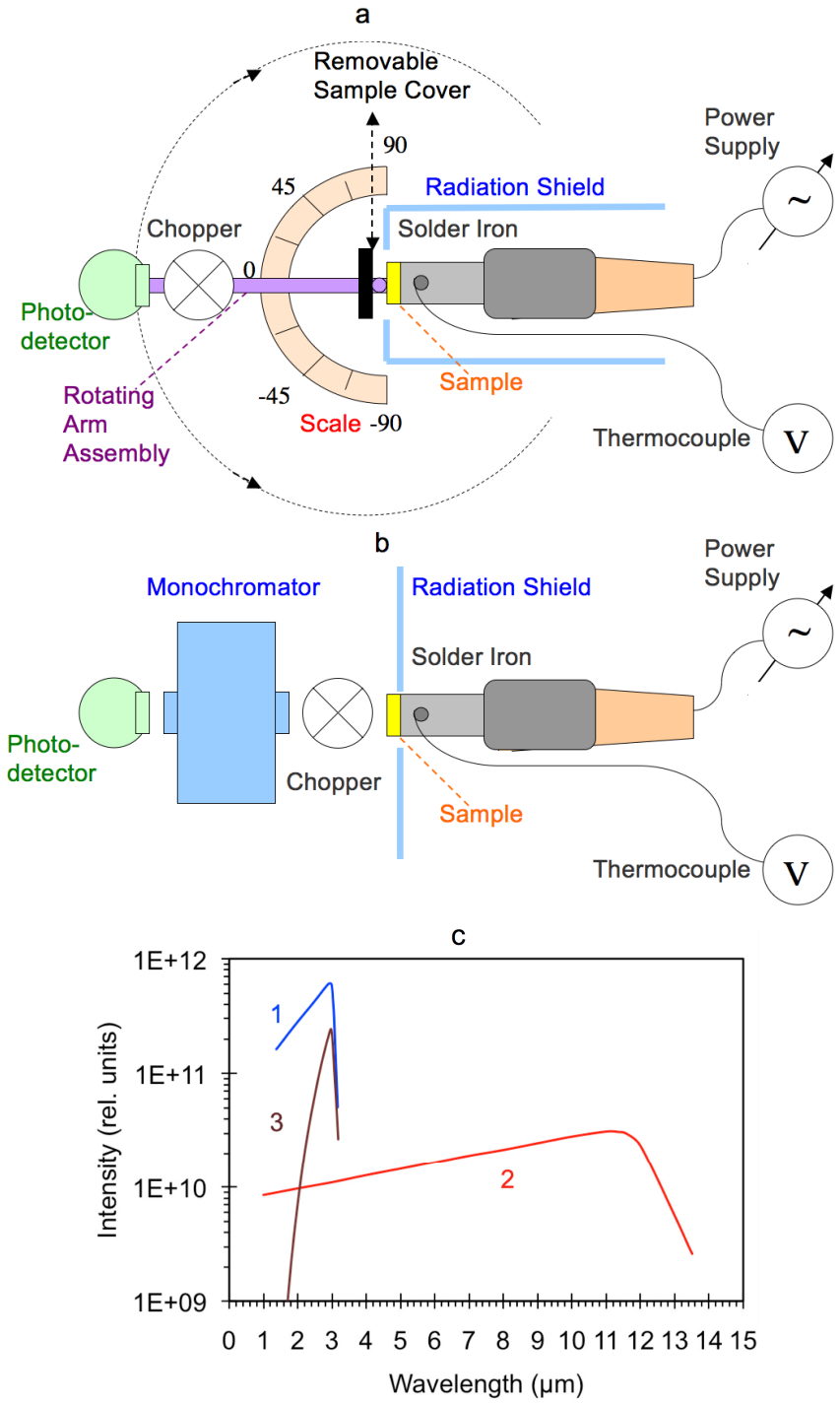

Fig. 1. (a) Schematics of angular emission measurements. (b) Schematics of spectral emission measurements. (c) Spectral sensitivity of the InSb (1) and HgTe (2) photo-detectors. Adopted from the manufacturer's (Hamamatsu) specification. (3) The product of the detector sensitivity spectrum and the blackbody radiation spectrum at T = 268 °C .

#231431 Received 24 Dec 2014; revised 12 Mar 2015; accepted 13 Mar 2015; published 4 Jun 2015

Although the drum helped to reduce the unwanted heat radiation dramatically, its base wall was still warm and produced residual parasitic thermal radiation noise. In order to take this unwanted radiation into account and further subtract it from the overall detected signal, we covered the tip of the solder iron with the 15 mm diameter cover (installed ~0.5 mm away from the flat end of the solder iron rod), which blocked radiation of the sample and practically did not disturb the thermal radiation of the cylinder's base wall, Fig. 1(a). Experimentally, we measured the thermal emission two times, with and without the cover and, by subtracting the former signal from the latter, obtained the emission radiated by the sample.

The thermal radiation was detected with the nitrogen cooled InSb photovoltaic detector from Hamamatsu (P5968-100), whose spectral sensitivity curve had a maximum at 2.95 μm, sharp drop at 3.1 μm, and the full width at half maximum (FWHM) equal to 1.0 μm, Fig. 2. At typical temperatures of the solder iron used in our experiments, the spectral thermal radiation intensity sharply dropped with the reduction of the wavelength. The product of the detector sensitivity spectrum and the blackbody radiation spectrum at T = 268 K (see the formula in Section 3.3) is shown in Fig. 2. The maximum of the resultant spectral profile is at 3.0 μm and FWHM is equal to 0.4 μm. Therefore, in the first approximation, the detected thermal radiation was quasi-monochromatic.

The detector was installed at the end of the arm that could be rotated in the horizontal plane about the axis coinciding (with ± 2 mm accuracy) with the center of the sample, Fig. 1(a). The height of the detector was equal to the height of the sample (with ± 2 mm accuracy) and the distance between the sample and the detector was equal to 255 mm. The optical chopper was installed on the same arm ~3 mm away from the detector. The arm with the detector and the chopper could be rotated from −90° to 90° (0° being the normal to the sample surface). All measurements were done in a dark room with lights turned off and other emission sources (like electronic displays and computer screens) dimmed or covered.

The electronic signal from the detector was amplified by the Tektronix TM 502A amplifier and recorded by the Tektronix TDS 784D oscilloscope that operated in the averaging regime, with the reference signal coming from the chopper.

2.5 Spectroscopic setup

Spectral measurements of the samples' emissivity in the forward direction (θ = 0) were carried out in the setup depicted in Fig. 1(b). The flat end of the solder iron rod with the deposited sample was positioned ~1 cm away from the wide open slit (~3 mm) of the monochromator (MS257 from Oriel) equipped with the grating, whose spectral range extended to 10 μm. The nitrogen cooled HgTe photodetector (P9697-01 form Hamamatsu), whose sensitivity spectral range extended from 1 μm to 13 μm (Fig. 1(c)), was attached to the exit slit of the monochromator. A thin aluminum plate (~10 cm x 10 cm) with the hole in the center, whose diameter was ~0.5 mm larger than the diameter of the solder iron rod, was used to transmit to the monochromator the thermal emission of the sample and shield the thermal radiation coming from other parts of the solder iron, Fig. 1(b). The optical chopper was placed between the sample and the monochromator slit. The temperature of the sample was monitored with the thermocouple as explained above. Two long pass filters (Ge, >1.7 μm) and (InAs, >3.5 μm) were used in corresponding spectral ranges to eliminate higher orders of diffraction. This allowed us to collect the thermal radiation within the 2 μm – 7 μm spectral range. The spectra were recorded with the use of the Merlin lock-in amplifier/control system. In order to calibrate our experimental setup (a combination of a monochromator, filter, and detector), we recorded at known temperature the spectrum of the black soot sample, whose thermal radiation spectrum closely approximated that of a blackbody [52].

#231431 Received 24 Dec 2014; revised 12 Mar 2015; accepted 13 Mar 2015; published 4 Jun 2015

3. Experimental measurements and results

3.1 Room temperature reflectance measurements

Reflectance of Au is well known and the reflectance of a lamellar metamaterial can be readily calculated knowing dielectric permittivities of constituent materials and film thicknesses. The purpose of the experiment described below was to experimentally study whether our Au films behave as predicted theoretically, based on the spectra of dielectric permittivities known from the literature.

In particular, we have studied angular reflectance profiles of the thick Au film (300 nm), looking for the well-known characteristic feature – a dip in the p polarized reflectance at the pseudo-Brewster angle [53]. The measurements were done in both p and s polarizations (as explained in Section 2.2) at $\lambda = 1.2$ μm and $\lambda = 2.0$ μm, Fig. 2. (Unfortunately, the wavelength range of our spectrophotometer did not extend to the maximum of the sensitivity curve of the InSb detector, $\lambda = 3.0$ μm, Fig. 1(c)).

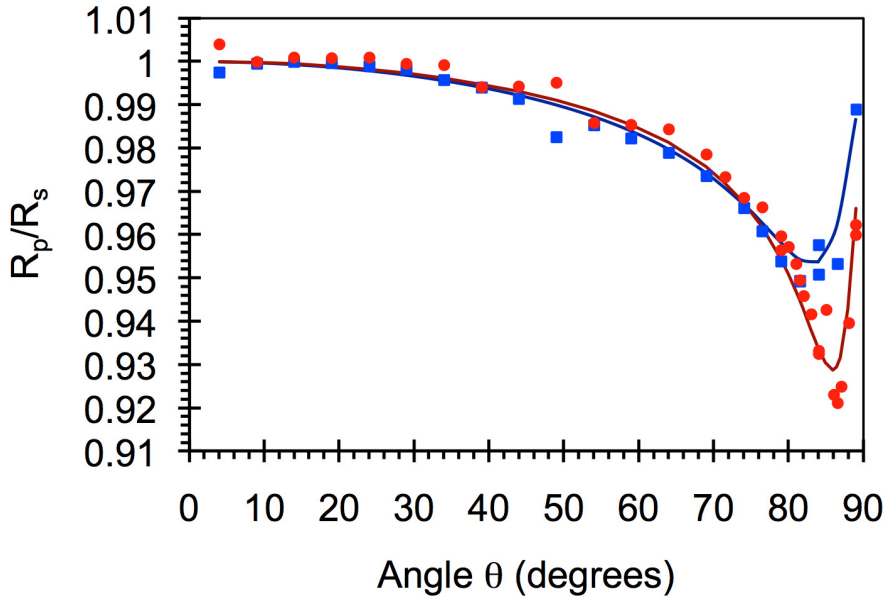

Fig. 2. Ratio of the p-polarized reflectance and s-polarized reflectance, $R(\theta)_p/R(\theta)_s$, measured in the 300 nm thick gold film. Red circles: experiment at $\lambda = 2$μm; blue squares: experiment at $\lambda = 1.2$ μm. Corresponding solid lines – theoretical fits, as explained in Section 4.1.

Due to complex interior relief of the of the integrating sphere, only ratios of reflectances in p polarization, $R(\theta)_p$, and s polarization, $R(\theta)_s$, could be measured with high accuracy. As follows from Fig. 2, these experimentally determined ratios, $R(\theta)_p/R(\theta)_s$, are in fairly good agreement with the ones predicted theoretically, as will be explained in Section 4.

3.2 Determining safe temperature range

In the first high temperature experiment, we studied thermal degradation of emitting surfaces in order to find the temperature range that was safe for the experimental samples. The temperature of the heater was ramped up with the rate of approximately 3.8 °C per minute, while the sample surface was monitored using the FLIRi7 thermal camera equipped with an external CaF_2 plane convex lens (focal length f≈40 mm). Although the camera was not designed to accurately measure the temperature of mirror-like surfaces, it was sensitive to changes of the thermal emissivity. As follows from Fig. 3, the temperature reading of the camera slowly increased with an increase of the actual temperature up to ~320 °C, after which

#231431 Received 24 Dec 2014; revised 12 Mar 2015; accepted 13 Mar 2015; published 4 Jun 2015

the temperature reading and the sample's emissivity increased abruptly. This increase was caused by thermal damage and tarnishing of the samples. (Thermal images of the Au sample before and after thermal degradation are depicted in inset of Fig. 3.) We have learned that at temperatures lower than 320 °C, no thermal damage occurred over one hour or longer, and we never exceeded this limit in our further experiments, whose duration ranged from ~10 min to ~30 min.

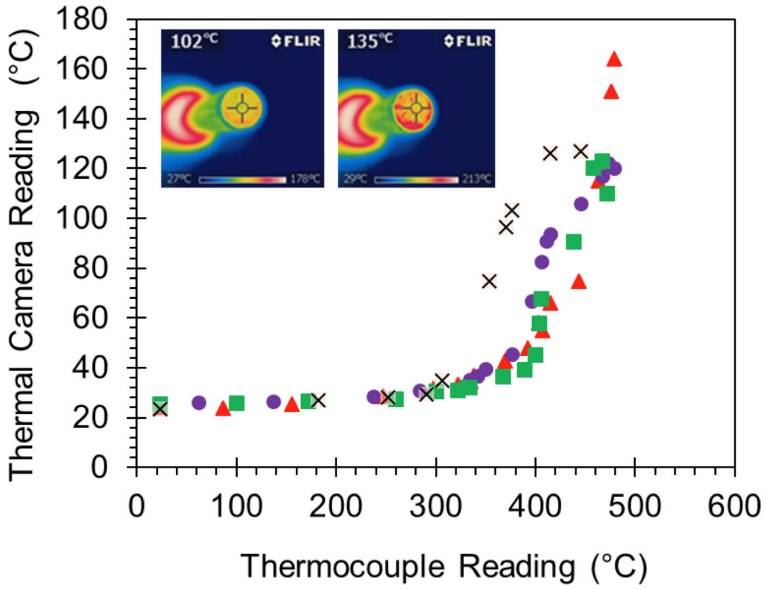

Fig. 3. Dependence of the temperature reading of the thermal camera plotted versus actual sample's temperature measured with the thermocouple for 150 nm thick Au film (purple circles), ~400 nm thick Au/MgF_2 lamellar metamaterial (red triangles), 270 nm MgF_2 film deposited on top of Cu (green squares), and Cu (black crosses). The temperature scan was 26 min long. Inset: Thermal image of the Au-coated flat end of the solder iron before (left) and after (right) thermal degradation.

3.3 Angular thermal emission measurements

Angular distribution of thermal radiation was measured in the setup of Fig. 1(a) (at $\lambda \approx 3$ μm, Fig. 1(c)) with the 5 degree step. For each sample, we collected two data sets, one with the cover in front of the sample (all background radiation, with the major contribution from the base wall of the drum) and one without the cover (emission of the sample plus all background radiation). By subtracting the former signal from the latter, we determined the angular distribution of the sample's thermal emission, Fig. 4(a). The measurements were repeated multiple times on multiple samples with the sample temperature ranging from ~170 °C to 315 °C. Depending on the sample and the temperature, the sample emission (in its maximum at $\theta = 0°$) could be as large as 300% or as small as 20% of the background radiation signal, causing large experimental noise in the latter case. All signals have been averaged over positive and negative angles (+ 5° and –5°, + 10° and –10°, etc.) in order to reduce the measurement noise and normalized to unity at the maximum. Angular distribution of thermal radiation of the black soot sample is plotted in Fig. 4(b) along with the function $\cos(\theta)$. One can see a good agreement between the experiment and the theoretical prediction – Lambertian function $\cos(\theta)$. The (random) measurement noise error was smaller than the size of the characters. Small deviation of the experiment from the model prediction could be due to some unaccounted systematic error, which has been accounted for in the calculation of the error bars in Fig. 4(c).

#231431 Received 24 Dec 2014; revised 12 Mar 2015; accepted 13 Mar 2015; published 4 Jun 2015

Angular distributions of thermal radiation of four Au samples measured at different temperatures are depicted in Fig. 4(c), along with the values averaged over four measurements (solid black circles). The error bars are shown for the averaged values as well as one particular data set, which has the largest error bars. Black solid line is the function cos(θ) and red and blue lines are the predictions of the directional form of the Kirchoff's law (as will be discussed in Section 4). One can see that in Au samples, the experimentally measured angular distributions of thermal radiation are closer to predictions of the Lambertian law, ∝cos(θ), than to the predictions of the Kirchoff's law.

Angular distributions of thermal radiation of Au/MgF_2 lamellar metamaterial (222 °C), Au with MgF_2 on top (225 °C), and Cu (230 °C) are depicted in Fig. 4(d). One can see that they follow the same general trend as the curves in Fig. 4(c) and do not exhibit any pronounced enhancement of thermal emission at the pseudo Brewster angle.

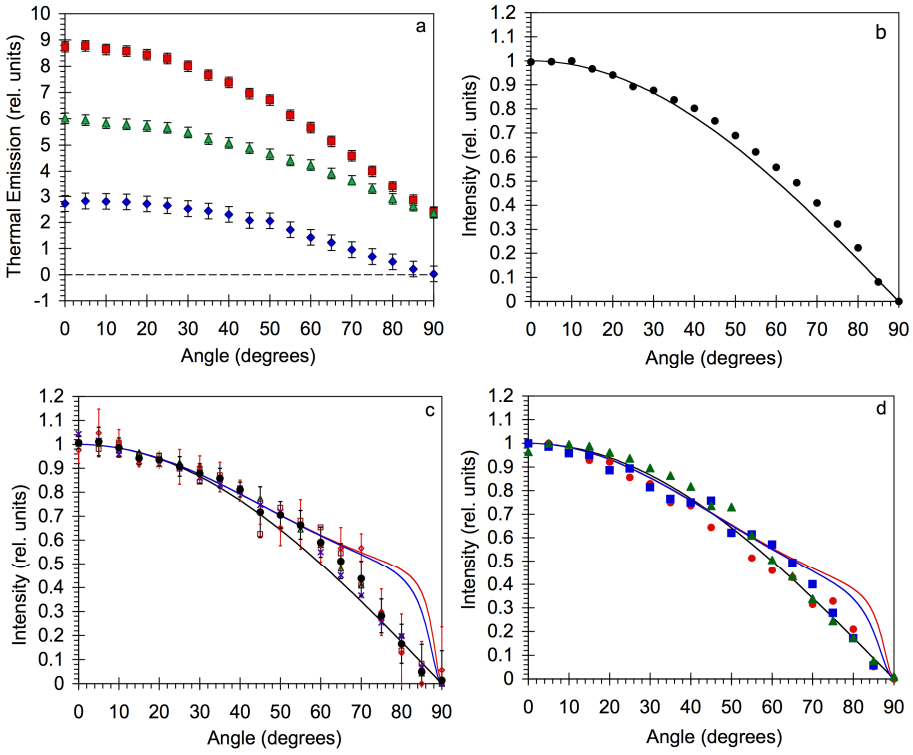

Fig. 4. (a) Trace 1 (red squares) – thermal emission of Cu sample and background (recorded without cover). Trace 2 (green triangles) – thermal emission of background (primarily radiation shield, recorded with cover). Blue diamonds – corrected thermal emission of Cu sample (Trace 3 = Trace 1 – Trace 2). (b) Angular distribution of thermal radiation of a black soot (at T = 225 °C) normalized to unity in the maximum. Solid line: Lambertian distribution, ∝cos(θ). (c) Angular distribution of thermal radiation of Au coated surfaces normalized to unity at θ = 0. Four independent measurements have been done at Au film thickness 100 nm, T = 315 °C (purple crosses, brown squares, and green triangles) and film thickness 130 nm, T = 223 °C (red diamonds). Solid black circles: average over the four measurements. The error bars are shown for the averaged data as well as for one particular data set with the largest error bars. Black line: cos(θ). Red line: sample absorbance calculated at λ = 3.0 μm from the p and s polarized reflectance spectra as A = [(2-R_s-R_p)/2]cos(θ). Blue line: same as above at λ = 2.0 μm. (d) Angular distribution of thermal radiation of Au/MgF_2 metamaterial (thickness ~400 nm, T = 222 °C, red circles), Au with MgF_2 on top (film thickness 80nm/80nm, T = 225 °C, blue squares), and Cu (T = 230 °C, green triangles). All signals are normalized to unity at the maximum. Black line: cos(θ). Red line: absorbance of the Au/MgF_2 metamaterial calculated at λ = 3.0 μm from the p and s polarized reflectance spectra as A = [(2-R_s-R_p)/3]cos(θ). Blue line: same as above at λ = 2.0 μm.

#231431 Received 24 Dec 2014; revised 12 Mar 2015; accepted 13 Mar 2015; published 4 Jun 2015

3.4 Spectral measurements of thermal emissivity

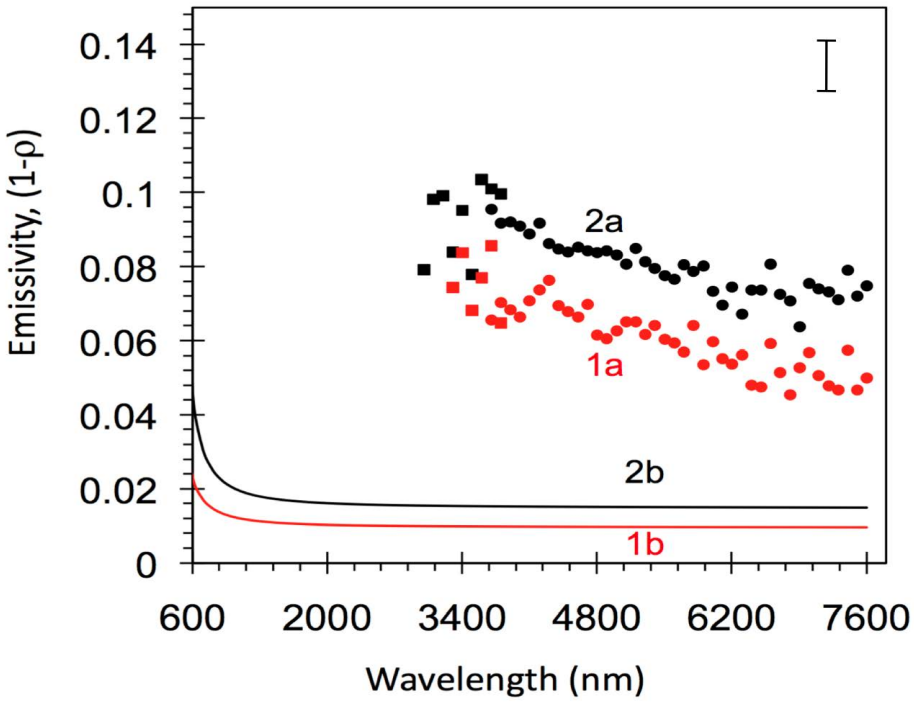

Fig. 5. Spectra of thermal emissivity of Au coated surface (film thickness 150 nm, T = 280 °C, trace 1a, red) and lamellar Au/MgF_2 metamaterial (thicknesses ~400 nm, T = 295 °C, trace 2a, black). Spectra of 1-ρ calculated for Au (1b) and lamellar Au/MgF_2 metamaterial (2b). The characteristic error bar is shown in the upper right corner.

Thermal emission spectra of the samples studied have been measured in the setup of Fig. 1(b) discussed above. All measurements were repeated at least two times to make sure that no sample degradation or the spectrum change happened in the course of the experiment.

Each experimental spectrum $I(\lambda)$ was assumed to be a product of the sample's emissivity $\varepsilon(\lambda)$, spectral sensitivity of the apparatus $S(\lambda)$, and the emissive power of a perfect black body $B(\lambda)$, $I(\lambda) = S(\lambda)B(\lambda,T)\varepsilon(\lambda)$. In the experiments, exactly in the same geometry, we recorded the emission spectrum of the sample to be studied $I_S(\lambda)$ and then the emission spectrum of a black soot $I_B(\lambda)$. By dividing the former by the latter, we have obtained the emissivity spectra of the samples as

$$\frac{I_S(\lambda)}{I_B(\lambda)} = \frac{S(\lambda)B(\lambda,T_S)\varepsilon_S(\lambda)}{S(\lambda)B(\lambda,T_B)\varepsilon_B(\lambda)} \quad \Rightarrow \quad \varepsilon_S(\lambda) = \frac{I_S(\lambda)B(\lambda,T_B)}{I_B(\lambda)B(\lambda,T_S)}\varepsilon_B(\lambda). \qquad (1)$$

The emissivity of the black soot $\varepsilon_B(\lambda)$ was assumed to be 96% in the whole spectral range [52]. When the spectra of the sample and the black soot were collected at the same temperature, the ratio of the two black body radiation spectra in Eq. (1) was simply equal to unity. However, when the two temperatures were slightly different (within ± 5°C), the theoretical blackbody emissive power spectra have been calculated and taken into account in Eq. (1) [54], (here λ is the wavelength, ν is the frequency, c is the speed of light, h is the Planck's constant, T is the temperature, and k_B is the Boltzmann's constant).

#231431 Received 24 Dec 2014; revised 12 Mar 2015; accepted 13 Mar 2015; published 4 Jun 2015

$$B(\lambda,T)=\frac{2hc^2}{\lambda^5}\frac{1}{\exp(hc/\lambda k_BT)-1} \quad \Leftrightarrow \quad B(\nu,T)=\frac{2h\nu^3}{c^2}\frac{1}{\exp(h\nu/k_BT)-1} \tag{2}$$

The resultant emissivity spectra of the Au film and Au/MgF_2 metamaterial are depicted in Fig. 5. The spectra are nearly flat and featureless, in agreement with the theoretical prediction, as will be discussed in Section 4. The thermal radiation spectra of Au film on top of MgF_2 film and MgF_2 film on top of Au film follow the same trend. However, their emissivity values are higher, probably due to poorer quality and higher absorbance.

4. Comparison of the experimental results with the model predictions

4.1 Effective medium dielectric permittivity of the lamellar metamaterial

The spectrum of the dielectric permittivity of gold $\varepsilon(\omega)$ was modeled with the Drude formula

$$\varepsilon(\omega)=\varepsilon_b-\frac{\omega_p^2}{\omega^2+i\omega\gamma}, \tag{3}$$

in which we first used the parameters adopted from Ref [55]. – the dielectric permittivity due to bound electrons was equal to ε_b = 9.00, plasma frequency was equal to ω_p = 1.37x10^{16} rad/s, and damping rate was equal to γ = 1.00x10^{14} rad/s.

Based on the spectrum of dielectric permittivity above and using the known Frensel formulas [53], we have calculated the angular reflectance profiles, $\rho(\theta)$, of semi-infinite Au slabs (good approximation to thick Au films) in p and s polarization and compared the calculated ratios $R(\theta)_p/R(\theta)_s$ to the experimental ones. We have found that the $R(\theta)_p/R(\theta)_s$ curves calculated using the Drude model parameters listed above (Ref [55].) have noticeable disagreement with the experiment. At the same time, a much better fit can be obtained at γ = 0.67x10^{14} rad/s, Fig. 2. This value (which is within a ballpark of that in Ref [56].) was used in our further calculations. The corresponding spectra of real and imaginary parts of dielectric permittivity of Au are shown in Fig. 6.

In the effective medium approximation, using the standard formula [57,58]

$$\begin{aligned}\varepsilon_{\parallel}&=f\varepsilon_m+(1-f)\varepsilon_d\\ \frac{1}{\varepsilon_{\perp}}&=\frac{f}{\varepsilon_m}+\frac{(1-f)}{\varepsilon_d}\end{aligned}, \tag{4}$$

we have calculated dielectric permittivities of the Au/MgF_2 lamellar metamaterial in the directions parallel, $\varepsilon_{\parallel}$, and perpendicular $\varepsilon_{\perp}$ to the layers, Fig. 6. (Here ε_m and ε_d are the dielectric permittivities of metal and dielectric, correspondingly, f is the filling factor of metal, and $\varepsilon=\varepsilon'+i\varepsilon''$.) In the calculations, we used the dielectric permittivities of gold discussed above, while MgF_2 was assumed to be lossless ε_d''=0 and dispersion-less, characterized by real part of dielectric permittivity equal to ε_d'=1.37^2=1.88 [59,60]. As one can see, $\varepsilon_{\parallel}'(\lambda)$ crosses zero at λ~470 nm. Correspondingly, the metamaterial has hyperbolic dispersion in the whole spectral range of interest, λ >1 μm.

#231431 Received 24 Dec 2014; revised 12 Mar 2015; accepted 13 Mar 2015; published 4 Jun 2015

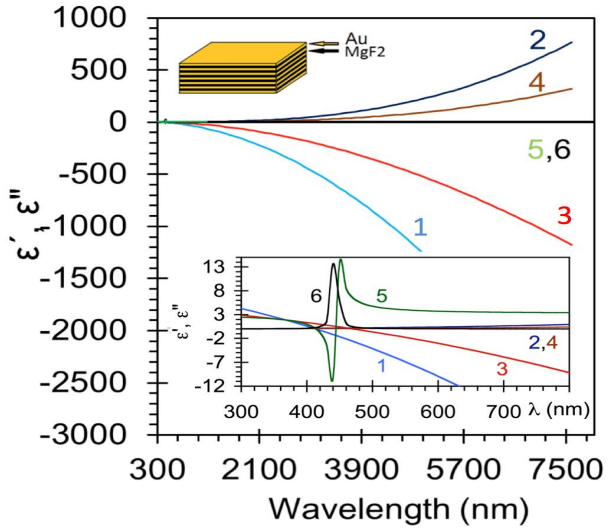

Fig. 6. Spectra of dielectric permittivity of Au (ε'- trace 1, ε''- trace 2), and lamellar metal/dielectric metamaterial ($\varepsilon'_{\parallel}$ - trace 3, $\varepsilon''_{\parallel}$ - trace 4, $\varepsilon'_{\perp}$ - trace 5, and $\varepsilon''_{\perp}$ - trace 6) in the directions parallel $\parallel$ and perpendicular $\perp$ to the layers. Upper inset: schematic of a lamellar hyperbolic metamaterial. Lower inset: Zoomed spectra of dielectric permittivities plotted in the main frame.

4.2 Angular distribution of thermal radiation

According to the directional form of the Kirchhoff's law, thermal emissive power $E(\theta,\lambda)$ radiated by an opaque body to a small solid angle in the direction of the polar angle θ (measured from the normal to the surface) is equal to absorptance $\alpha(\theta,\lambda) = 1-\rho(\theta,\lambda)$ (where $\rho(\theta,\lambda)$ is reflectance) multiplied by the thermal emissive power of a black body $B(\theta,\lambda)\propto\cos(\theta)$. The reflectance of a uniaxial metamaterial sample can be calculated using the known formula [61]

$$\rho(\lambda)=|r|^2=\begin{cases}\left|\dfrac{\sin(\theta-\theta_t)}{\sin(\theta+\theta_t)}\right|^2, & \theta_t=\arcsin\left(\dfrac{\sin\theta}{\sqrt{\varepsilon_{\parallel}}}\right), \quad s\text{ polarization.}\\ \left|\dfrac{\varepsilon_{\parallel}\tan\theta_t-\tan\theta}{\varepsilon_{\parallel}\tan\theta_t+\tan\theta}\right|^2, & \theta_t=\arctan\sqrt{\dfrac{\varepsilon_{\perp}\sin^2\theta}{\varepsilon_{\parallel}\varepsilon_{\perp}-\varepsilon_{\parallel}\sin^2\theta}}, \quad p\text{ polarization.}\end{cases}. \quad (5)$$

The calculated reflectance spectra, $\rho(\theta)$, of Au and Au/MgF_2 metamaterial samples featuring a dip at the pseudo Brewster angle in p polarization, are shown in Fig. 7. In order to compare the theoretical prediction with the result of the unpolarized thermal radiation experiment, the average should be taken over p polarized and s polarized emission components. Such curves, calculated for λ = 2.0 μm (blue line) and λ = 3.0 μm (red line) and normalized to unity in the maximum, are plotted in Figs. 4(c) and 4(d), along with the experimental data. Black solid line in the same figures represents the Lambert's law, ∝ cos(θ). One can see, that despite of tendency of some experimental points to rise above the cos(θ) curve, there is a quantitative disagreement between the experimental results and the predictions of the Kirchhoff's law.

#231431 Received 24 Dec 2014; revised 12 Mar 2015; accepted 13 Mar 2015; published 4 Jun 2015

This result is not unique to Au and Au/MgF_2 lamellar metamaterial surfaces. Thus, angular distribution diagrams of thermal radiation measured in the Au film coated with the MgF_2 film, and bare Cu surface are qualitatively similar to that of Au and metamaterial (compare Figs. 4(c) and 4(d)) and different from the predictions of the Kirchoff's law.

Note that the theoretical curves calculated for $\lambda = 2.0$ μm and $\lambda = 3.0$ μm are close to each other (Figs. 4(c), 4(d)) and the conclusions above are valid for both wavelengths, one corresponding to the spectral maximum of the detected signal (Fig. 1(c)) and the second – off by more than two FWHM widths. This makes our conclusions robust to lack of pure monochromaticity of the detected signal and possible uncertainty in the precise knowledge of the dielectric permittivity of gold.

4.3 Thermal radiation spectra

The calculated normal incidence reflectance spectra of Au and Au/MgF_2 metamaterial are plotted as $1\text{-}\rho(\lambda)$ vs λ in Fig. 5. Following the Kirchoff's law, $1\text{-}\rho(\lambda)$ is associated with the thermal emissivity $\varepsilon(\lambda)$ (at $\cos(\theta) = 1$). As follows from Fig. 5, in the experiment and in the calculation: (i) the emissivity $\varepsilon(\lambda) = 1\text{-}\rho(\lambda)$ of the Au/MgF_2 metamaterial is slightly larger than that of Au, and (ii) at 3 μm < λ < 7 μm, the emissivity spectra $\varepsilon(\lambda) = 1\text{-}\rho(\lambda)$ of both Au and Au/MgF_2 metamaterial are featureless, experiencing slight increase toward shorter wavelengths. Since in both Au and Au/MgF_2 metamaterial $\rho(\lambda) \approx 1$, the small difference $1\text{-}\rho(\lambda)$ is inherently highly sensitive to sample imperfections (absorption loss) as well as small systematic measurement errors. Therefore, we conclude that both experimental emissivity and experimental absorptance $1\text{-}\rho(\lambda)$ qualitatively follow the theoretically predicted trends and their modest quantitative disagreement is well understood.

5. Summary and discussion

To summarize, we have studied thermal radiation of several metallic and metal/dielectric surfaces, including Au and lamellar Au/MgF_2 metamaterial with hyperbolic dispersion.

The experimental spectra of thermal radiation (measured at $\theta = 0$) qualitatively resemble the theoretically predicted ones. A modest quantitative disagreement between the model and the experiment can be explained by inherent strong sensitivity of the small difference $1\text{-}\rho(\lambda)$ to variations of $\rho(\lambda)$.

We have shown that angular emission diagrams of the metal and metal/dielectric samples studied deviate from the prediction of the directional Kirchoff's law and, in many cases, closely follow the Lambert's law, $\propto\cos(\theta)$, Figs. 4(c) and 4(d). This is the central result of this work.

The angular distributions and the spectra of thermal radiation of hyperbolic metamaterials and pairs of Au and MgF_2 layers were qualitatively similar to those of simple metallic surfaces, such as Au or Cu. In the mid-infrared part of the spectrum, negative real values of dielectric permittivity of gold and Au/MgF_2 metamaterial with hyperbolic dispersion (in the direction parallel to the surface) are very large. Therefore, many features in the experimental behavior of hyperbolic metamaterials can be expected to be similar to those of bulk metals.

Deviation of the angular distribution of thermal radiation of metallic and metal/dielectric surfaces from the prediction of the directional form of the Kirchoff's law deserves a separate comment. First of all, the Kirchoff's law is formulated for materials radiating and absorbing in thermodynamic equilibrium with the environment – the condition, which is, strictly speaking, not satisfied in open systems, like our experiment. Therefore, we are examining the Kirchoff's law outside the range of its applicability (which a common practice in the literature). Second, several publications [27,62] analyzing the directional form of the Kirchoff's law, linked it to the reciprocity and the time-reversal symmetry, and pointed out at several systems (including multilayer stacks and materials with large imaginary part of the dielectric constant), in which the law may be violated. We hope that our findings will stimulate new theoretical studies of this intriguing phenomenon.

#231431 Received 24 Dec 2014; revised 12 Mar 2015; accepted 13 Mar 2015; published 4 Jun 2015

Acknowledgments

The authors acknowledge NSF PREM grant DMR 1205457, NSF IGERT grant DGE 0966188, NSF HBCU RISE grant HRD-1345215, ARO grant W911NF-14-1-0639, ARO MURI, NSF Center for Photonics and Multiscale Nanomaterials, and Gordon and Betty Moore Foundation.

#231431 Received 24 Dec 2014; revised 12 Mar 2015; accepted 13 Mar 2015; published 4 Jun 2015